# Microplasma discharge-based nitrogen fixation driven by triboelectric nanogenerator towards self-powered mechano-nitrogenous fertilizer supplier

*Man-Chung Wong, Wei Xu, Jianhua Hao**

Department of Applied Physics, The Hong Kong Polytechnic University, Hong Kong, P. R. China
E-mail: jh.hao@polyu.edu.hk

**Keywords:** triboelectric nanogenerators, self powered devices, nitrogen fixation, mechanical energy harvesting

## Abstract

Development of novel nitrogen fixation technology is realistically significant for fertilizer industry and agriculture. Traditional plasma-induced nitrogen fixation technology is severely limited in some occasions because this route generally requires a continuous power input with the features of complicated apparatus fabrication, high cost and non-portability, etc. Herein, we conceive a triboelectric nanogenerator (TENG)-driven microplasma discharge-based nitrogen fixation system by integrating a high voltage output TENG and a discharge reactor. The novel TENG has the capability to generate high voltage of about 1300 V without additional auxiliary. The generated voltage can induce microplasma discharge under atmospheric environment in the discharge reactor, where nitrogen gas is successfully converted into nitrogen dioxide and nitric acid, and the atmospheric nitrogen fixation is therefore realized. The TENG-driven microplasma discharge-based nitrogen fixation system can serve as a nitrogenous fertilizer supplier, and correspondingly, $NaNO_3$ fertilizer is produced via driving the system by human walking stimuli for crop cultivation. This study offers a promising atmospheric nitrogen fixation strategy with energy-saving, environmental friendliness, flexible operation, and high safety.

## 1. Introduction

The progress of life on earth requires continuously and large amount of nitrogen ingestion because nitrogen is an essential and indispensable building block for life.[1-2] Even though there is considerable nitrogen surplus in earth atmosphere, this molecular nitrogen cannot be absorbed directly by most organisms because of the high activation energy.[3] Therefore, to develop nitrogen fixation technology, the conversion of nitrogen in air to a biologically usable nitrogenous compounds, is realistically significant for the development of fertilizer industry and agriculture. Inspired from the natural lighting nitrogen fixation, plasma-induced nitrogen

fixation can ionize air to produce the nitrogen oxide and other nitrogen compounds for further fertilizer synthetization, and possesses a series of advantages, such as abundant raw material source and zero greenhouse gas emission etc. Among them, the gliding arc plasma is considered as one of the most effective and promising plasma sources for nitrogen fixation or other gas conversion because of its excellent energy deliver efficiency and yield.[3-4] However, these nitrogen fixation routes have to require a continuous and huge power input for generating plasma,[5] which aggravates energy shortage in modern society. Additionally, some features in common plasma-induced nitrogen fixation, such as the complicated apparatus fabrication, high cost and non-portability etc., also pose a challenge to its further application. [6-7]

Recently, triboelectric nanogenerator (TENG), a novel technology converting mechanical energy into electricity, is attracting a wide attention.[8-13] The device's operation is mainly based on the triboelectricity and electrostatic effects.[14-17] Specifically, as the TENG is driven by mechanical stimuli, the contact of two dissimilar materials enables the contact electrification ascribed to the two contact surfaces because of their difference in tendencies to gain or lose electrons.[18-19] The subsequent separation of the two oppositely charged surfaces will generate an electric potential difference for TENG voltage output. Hence, the mechanical energy is harvested and converted into electricity. This unique working principle endows TENG with a series of advantages, such as simple device structure, ease of fabrication process, versatile material choice, the abundant availability of targeting mechanical energy and so on, to overcome obstacles in traditional energy supply source utilized in nitrogen fixation.[20-26] Meanwhile, the high efficiency in low contact frequency enables TENG to make full use of the natural, widely distributed, and long-term ignored ambient mechanical energy for electric generation,[12, 27-32] which makes TENG become an energy-saving, environmental-friendly and low-cost electricity supply source.[33-34] Moreover, TENG's intrinsic feature of high voltage and low current is also suitable for inducing microplasma discharge. In these regards, integrating TENG as a high voltage source into microplasma discharge-based nitrogen fixation is a feasible and ideal strategy, which deserves more attempt. Even though a few TENGs with high voltage output have been exploited as the power source for various occasions, such as mass spectrometer, electroluminescence device, optical gating, and electrospinning etc..[35-41], there is rarely report related to TENG directly driving atmospheric microplasma discharge and still less its application in nitrogen fixation field. Additionally, current TENGs generally require explicit operation conditions, such as high frequency of mechanical stimuli, unfeasible stress or a customized situation,[42-44] and complementary auxiliary, such as additional voltage sources for hybridization and voltage multiplier circuit, etc.,[35, 39, 45] for achieving a reliable

high voltage output. Thus, it is more necessary and significant to develop a high voltage TENG with simplified operation and structure for further application.

In this study, we developed a TENG-driven microplasma discharge-based nitrogen fixation system (TENG-microplasma nitrogen fixation system) by integrating a TENG and an microplasma discharge reactor. The TENG with simple structure was designed based on our evaluation in contact electrification ability of materials and was prepared using polyurethane (PU) foam and ebonite sheet as contact materials. It could provide a high voltage output of about 1300 V and a low current output of about 60 μA driven by mechanical stimuli. The generated voltage is directly applied on electrodes of the discharge reactor for atmospheric microplasma discharge, where the nitrogen gas in air is successfully converted into nitrogenous compound, including nitrogen dioxide and nitric acid solution. We further employ the TENG-microplasma nitrogen fixation system as a nitrogenous fertilizer supplier. Consequently, fertilizer ($NaNO_3$) is achieved via driving the system by human walking stimuli to benefit the plant cultivation. This work provides a feasibility to develop an energy-saving, environmental-friendly, flexible, and safe nitrogen fixation route.

## 2. Result and discussion

The structural design of the TENG-microplasma nitrogen fixation system is shown in Figure 1a and 1b. This system consists of two parts, namely a contact-separation mode TENG with high voltage output and a microplasma discharge reactor for nitrogen fixation. The TENG is illustrated in Figure 1c (i), including a PU foam and an ebonite sheet as top and bottom frictional layers, respectively. Two nickel (Ni) films were deposited on the surface of the two-contact layer and performed as electrodes for electric output of the TENG, and polycarbonate was used as the substrate of the device. For the microplasma discharge reactor, it is considered as an air-filled miniature glass cylinder. Two stainless steel needles, acting as the discharge electrodes, are fixed at the interior of the glass cylinder as shown in Figure 1c (ii). The needle electrodes are directly connected to the TENG, and thus the voltage generated by TENG can be applied between two needle electrodes for microplasma discharge. Some DI water was placed at the bottom of glass cylinder to absorb generated nitrogen compounds during the process of microplasma discharge.

The working mechanism of the TENG-microplasma nitrogen fixation system is shown in Figure 1d. For each operating cycle of TENG, PU foam and ebonite are brought into physical contact. According to the triboelectric series of materials' tendency to gain or lose electrons, electrons are transferred from the PU foam into ebonite at the interface, and these two surfaces

are charged with opposite polarities. When they are parted, a difference in electric potential is produced between the two Ni electrodes. Subsequently, when the two separated charged frictional layers are gradually brought together again, a voltage output with reversed polarity is generated. The output voltages are applied between the two needle electrodes in the microplasma discharge reactor. The voltage across the needle will thereby change with the gradual contact or separation of the frictional layers. Once this voltage exceeds the dielectric strength of air, ionization of air molecules and microplasma discharge will be occurred in the region between needle electrodes, enabling nitrogen to be transformed into nitrogen compounds. By means of this process, the ambient mechanical energy is harvested to generate electricity for microplasma discharge-based nitrogen fixation.

The TENG plays an important role in the operation of the TENG-microplasma nitrogen fixation system. It harvests and converts ambient mechanical energy into electricity, and therefore serves as a power source to drive the system. In order to evaluate the performance of the prepared TENG, a device with the size of 25 $cm^2$ was fabricated for the performance measurement. The results show that the TENG can provide a high voltage output. As shown in Figure 2a and 2b, triggered by an impulsive force of 70 N, the open-circuit voltage ($V_{oc}$) and the short-circuit current ($I_{sc}$) of TENG are capable of reaching up to about 1300 V and 60 μA, respectively. Meanwhile, the dependence of peak instantaneous output current and power on the external loads are also studied as shown in Figure 2c. It is found that the increased load resistance leads to the instantaneous current drops, and correspondingly, the peak instantaneous power of the TENG reaches a maximum of 27 mW at a load resistance of 100 MΩ. This means that the maximum instantaneous power density is 0.432 $W/m^2$. The high electric output is mainly attributed to the significant difference in electron affinity between the PU foam and ebonite, which increases the amount of separated charges during the TENG operation and results in a high voltage output. Additionally, compared with the flat structure, the porous structure of the utilized PU foam can lead to an enhanced effective contact area between frictional materials, which contributes to the high electric output of TENG as well.

Figure 2d shows the effect of pore sizes of PU foam on the electric output of the device. PU foam is generally regarded as an excellent triboelectric charge donor. Previous studies suggest that its output performance as a TENG frictional layer can be further refined.[46-47] We expect that the pore size of the foam adapts a critical role of triboelectric charging in a vertical contact-separation mode. It is found that the $V_{oc}$ obviously increases when the pore size increases from 0.25 mm to 0.61 mm. As aforementioned, during the operation of TENG, PU foam layer will be periodically compressed and released with contact and separation of the two

frictional layers. The larger pore size may be beneficial for forming an improved effective contact area between frictional materials accompanying the compression of PU foam, leading to the enhancement in the device's performance. On the other hand, the hardness of PU foam will decrease with an increase in the pore size. This reduces the resistance for the device's operation and may assist the contact area between frictional layers to become larger. Therefore, the $V_{oc}$ obviously increases with the enlargement of the pore size of PU foam, and the peak $V_{oc}$ of about 1300 V is obtained as the PU pore size is about 0.61 mm. Nonetheless, as further increase in the pore size to above 3 mm, the proportion of PU in whole foam will become too small as shown in Figure 2d, which causes significant decrement of the effective contact area and the electric output of device. Therefore, we employ the PU foam with pore size of 0.61 mm as an optimized friction layer for further device fabrication. Figure 2e presents the relationship between the open-circuit voltage and the size of frictional layers in the prepared TENG. It can be observed that the $V_{oc}$ proportionally increases from 500 V to more than 2200 V when the friction layer area varies from 9 to 100 $cm^2$. Moreover, we also conducted a durability test of device as shown in Figure 2f. It is found that after a continuous operation of 50000 cycles, no significant distortion or serious damage on the frictional layers is observed via comparing the morphologies of the two friction layers before and after operation. As a result, the electrical output of device remains stable during the process and the fluctuation of $V_{oc}$ is less than ±0.3% (with a fixed frequency of 7 Hz). The ultra-high electric output and great reliability of the prepared TENG enable it to be a good voltage supply source for TENG-microplasma nitrogen fixation system.

In TENG-microplasma nitrogen fixation system, the output voltage generated by TENG will be directly applied to the needle electrodes in discharge reactor for microplasma discharge. As shown in Figure 3a, the microplasma discharge has been successfully observed during TENG operation. The detailed discharge process can be further analyzed by studying the change of voltage ($V_c$) and current ($I_c$) between needle electrodes. Figure 3b illustrates the $V_c$ and $I_c$ during 4 operation cycles of TENGs, and the gap distance between needle electrodes is 0.2 mm. Taking one cycle as an example, it can be observed that $V_c$ initially increases up to a discharge voltage of ~1500 V and suddenly decreases to 0 V (Fig 3b (i)). Simultaneously, $I_c$ grows rapidly to a discharge current of about 300 μA (Fig 3b (ii)). This means that the applied electric field causes air between the needle electrodes to generate electrical breakdown and induce immediate charge transfer through the air gap. Subsequently, the $I_c$ decreases back to 50 nA within 0.002 s, and $V_c$ starts to gradually increase due to the continuous electric supply from the TENG as well as the remaining charges in needle electrodes. When the $V_c$ reaches up

to 1000 V, the second discharge occurs in the same half cycle. It is noticed that the discharge phenomenon happens only in the positive half cycles, and there is no microplasma discharge in the negative half cycle. That is because a plasma discharge generally requires a threshold voltage. According to Paschen's curve,[48] when the separation of electrode gap is 0.2 mm and the operating pressure is 1 atm, the threshold voltage is about 1000 V. However, the maximum output voltage of TENG in negative cycle is around 500 V as shown in Figure 3b (i), which is thereby incompetent to generate another discharge. The released energy for each microplasma discharge is an important parameter characterizing the microplasma itself. It can be quantitatively analyzed by the voltage-charge-cyclogram, namely Lissajous figures. Figure 3c illustrates the Lissajous figures of the microplasma discharge process. The released energy for each microplasma discharge ($E_L$) can be calculated as

$$E_L = \int Q \cdot dV = A_{Lissajoous} \tag{1}$$

where $Q$ is transferred charge during microplasma discharge, and $V$ is the $V_c$ during microplasma discharge, $A_{\text{Lissajoous}}$ is the area of the enclosed curve.

The results show that for each microplasma discharge with a gap distance of 0.2 mm, the $E_L$ is calculated as about 0.14 μJ. According to the statistical results in Figure 3b, about 1.75 discharges are observed in per operation cycle of TENG. This means that the average released energy ($E_{ave}$) during discharge per cycle is about 0.26 μJ.

The gap distance between needle electrodes plays an important role in the microplasma discharge process. Figure 3d shows the changes in $V_c$ and $I_c$ during the discharge process with the gap distance of 0.6 mm. The results show that compared with the microplasma discharge with the gap distance of 0.2 mm, the amount of microplasma discharges statistically decreases to about 0.3 times per operation cycle. Meanwhile, during the microplasma discharge, the discharge voltage increases to about 2 kV, while the discharge current decreases to 287 μA. That is because such a wide gap distance (0.6 mm) would limit the formation of a conductive path between needle electrodes via ionization of air molecules, leading to a higher threshold voltage, a smaller discharge current, and reduced number of microplasma discharges for each operation cycle. In addition, the released energy for each microplasma discharge $E_L$ with the gap distance of 0.6 mm is measured based on the Lissajous figures as shown in Figure 3e. The results reveal that the $E_L$ from this discharge is about 0.19 μJ. Correspondingly, the average discharge energy per operation cycle ($E_{ave}$) is 0.16 μJ, which is comparatively lower than that of the microplasma discharge with the gap distance of 0.2 mm. In order to optimize the TENG-driven microplasma discharge process, the dependence of discharge voltage, discharge current,

$E_L$ and $E_{ave}$ on the gap distance is summarized in Figure 3f and Figure 3g, respectively. It can be observed that the discharge voltage and $E_L$ increase while the discharge current decreases with gap distance enhancement. Correspondingly, the average released energy $E_{ave}$ arrives at maximum of 0.28 μJ when the discharge gap distance is about 0.3 mm, whereas more ionized gas is generated to benefit the microplasma discharge and nitrogen fixation.

Through the microplasma discharge driven by TENG, nitrogen in the air will be converted into nitrogen compound for accomplishing nitrogen fixation. The related reactions are summarized in Figure 4a. Particularly, during the microplasma discharge process, the high electric field strength between needle electrodes excites these nitrogen and oxygen atoms in the air between needle electrodes. This excitation generates high energy electrons and causes molecular $N_2$ and $O_2$ to be dissociated into nitrogen and oxygen free radicals, as shown in the following equations: [49-52]

$$O_{2(g)} + e^- \rightarrow 2O_{(v)} + e^- \quad (2)$$

$$N_{2(g)} + e^- \rightarrow 2N_{(v)} + e^- \quad (3)$$

These free radicals further lead to the generation of nitrogen oxides by different reaction routes. Among them, the essential reactions can be considered as: [3, 49-52]

$$N_{(v)} + O_{(v)} \rightarrow NO_{(g)} \quad (4)$$

$$NO_{(g)} + O_{(v)} \rightarrow NO_{2(g)} \quad (5)$$

The synthesized nitrogen oxides are then collected via dissolving them into DI water placed in the discharge reactor, forming nitric acid and complete the nitrogen fixation, as shown below: [53]

$$4NO_{2(g)} + 2H_2O_{(l)} + O_{2(g)} \rightarrow 4HNO_{3(aq)} \quad (6)$$

$$3NO_{2(g)} + H_2O_{(l)} \rightarrow 2HNO_{3(aq)} + NO_{(g)} \quad (7)$$

To provide more evidence concerning these reactions, we firstly analyze the emission spectrum of the discharge microplasma as shown in Figure. 4b. The characteristic emission peaks of the dinitrogen and nitrogen free radical are observed, indicating the dissociation of dinitrogen molecules. To verify the subsequent generation of nitrogen oxides from the recombination of free radicals, we further investigate the concentrations profile of nitrogen dioxide ($NO_2$) at different sampling distance (Figure 4c). Herein, the sampling distance is defined as the length between the discharge and the probe of a gas sensor (EDKORS ADKS-1) as shown in Figure 4d. The results demonstrate that the $NO_2$ concentration increases with the decrement of sampling distance. This phenomenon confirms that $NO_2$ is generated during the microplasma discharge. In addition, we also measured the effect of gap distance between

needle electrodes on the amount of produced $NO_2$. As shown in Figure 4e, it is interesting to notice that the concentration of $NO_2$ in microplasma discharge reactor reaches a maximum value when the gap distance is 0.3 mm. This is because the highest average discharge energy $E_{ave}$ is arrived in this case as shown in Figure 3g, which means that more ionized gas is generated during this discharge process to obtain the maximum amount of $NO_2$. It should be pointed out that there is no nitric oxide (NO) detected in the reactor, which may be attributed to the rapid oxidation of generated NO into $NO_2$. The generated $NO_2$ is supposed to be dissolved into water to form the nitric acid solution, and its Raman spectrum after 12000 operation cycles is exhibited in Figure 4f. Herein, the strong emission bands at 1046 $cm^{-1}$and at 688 $cm^{-1}$ are observed, which correspond to the symmetric stretching $\nu_{1s}$ $NO_3$ vibration and the $NO_2$ bending δ O-N-O mode vibration, respectively. Moreover, a minor shoulder peak can be observed at 929 $cm^{-1}$ and 1304 $cm^{-1}$, which are attributed to ν N-(OH) and $\nu_s$ $NO_2$ vibration modes, respectively. Based on the previous reports,[54] it is reasonable to deduce that nitric acid has been successfully synthesized via TENG-driven microplasma discharge. It is noticed that the nitrate concentration in nitric acid increases with the extended operation time of the nitrogen fixation system as illustrated in Figure 4g. The peak nitrate concentration of about 250 ppm is arrived when the operation time and gap distance are 400 min and 0.3 mm, respectively. Even though the energy efficiency of the TENG-microplasma based nitrogen dioxide synthesis is lower than that of Haber Bosch process and gliding arc-based nitrogen oxide synthesis (37.1 MJ/mol),[3] this novel strategy still processes unique advantages whereas other methods lacked. Especially, the TENG-microplasma nitrogen fixation can harvest ambient and ignored mechanical energy to realize *in-situ* nitrogen fixation, which benefits relieving energy shortage.

The generated nitric acid can be utilized in various fields, and its primary consumption is for the synthesis of nitrogenous fertilizer, including $NaNO_3$, $NH_4NO_3$ and $CaNO_3$, etc. These synthetic nitrogenous fertilizers are essential for agricultural development. Figure 5a and 5b demonstrate an application scenario of the TENG-microplasma nitrogen fixation system as the sustainable, environmental-friendly and safe *in-situ* nitrogenous fertilizer supplier. Specifically, in the system, a TENG with the area of 64 $cm^2$ is covered with artificial turf and then buried inside a pot hole (highlighted with the blue blanket in Figure 5a and 5b). Once the TENG is triggered by the ambient mechanical stimuli, such as human walking, the mechanical energy will be harvested and converted into electricity, and the output $V_{oc}$ can reach up to above 1000 V as shown in Figure 5c. This output voltage is applied between two needle electrodes inside the microplasma discharge reactor (highlighted with the yellow blanket in Figure 5b) for the microplasma discharge and the generation of $NO_2$. With regarding to safe and direct *in-situ*

nitrogenous fertilizer fabrication, weak sodium bicarbonate solution was placed inside the discharge reactor to absorb and react with the generated $NO_2$ for forming the sodium nitrate ($NaNO_3$) solution as fertilizer. Figure 5d illustrates the Fourier-transform infrared spectroscopy (FTIR) analysis of the solution, and the transmittance characteristic peak of N-O stretching vibration group is found in the wave numbers of 1290 $cm^{-1}$, 2431 $cm^{-1}$and 875 $cm^{-1}$,[55] which confirms the successful preparation of $NaNO_3$. As a demonstration, these synthesized $NaNO_3$ are utilized as fertilizers to benefit the growth of green bean. We compared the green bean samples with and without the addition of $NaNO_3$ fertilizers generated by TENG-microplasma nitrogen fixation system. The results reveal that after the growth for one week, the fresh weight of total biomass (leaves, stems, and roots) of the sample with $NaNO_3$ addition is 1.4-fold heavier than that of the sample without $NaNO_3$, as shown in Figure 5e. This indicates the feasibility and application potential of the self-powered TENG-microplasma nitrogen fixation system as the mechano-nitrogenous fertilizer supplier. Compared to the other nitrogen fixation technologies, such as traditional Haber Bosch process or plasma based process, the TENG-microplasma nitrogen fixation system makes full use of the dissipated, ignored and wasted ambient mechanical energy for the synthesis of nitrogen compounds and therefore possesses the unique features of energy-saving and environmental-friendliness. Meanwhile, the TENG-microplasma nitrogen fixation system also avoids the operation environment of high temperature and high pressure in Haber Bosch process, leading to the better safety of the system. Additionally, the low cost and simplicity of our system contributes to an improved portability and usability for practical application. Therefore, the self-powered TENG-microplasma nitrogen fixation can be considered as an attractive alternative to traditional nitrogen fixation technology. The detailed comparison between the TENG-microplasma nitrogen fixation and the other nitrogen fixation technologies is summarized in Table 1. It is hoped that the proposed nitrogen fixation system paves a way to prepare the nitrogen compound from air in an energy-saving, environmental-friendly, flexible, and safe way.

## 3. Conclusion

In summary, a TENG-driven microplasma discharge-based nitrogen fixation system has been developed by integrating a high voltage output TENG with a microplasma-discharge reactor. Based on the maximized electron affinity difference between contact materials and the optimized pore sizes of PU foam, the TENG can output a steady high voltage of about 1300 V driven by mechanical stimuli without any auxiliary. The generated voltage is directly applied between needle electrodes of the discharge reactor for atmospheric microplasma discharge, and

the effect of gap distance on discharge process, including discharge voltage, discharge current and average discharge energy per TENG operation cycle have been systematically investigated. It is observed that the nitrogen gas in air can be successfully converted into nitrogen compound, including nitrogen dioxide and nitric acid solution, via the TENG-driven microplasma discharge process to finally realize the nitrogen fixation. The $NO_3^-$ concentration of 250 ppm can be arrived after continuously operating the TENG for 400 min. Furthermore, we employ the TENG-microplasma nitrogen fixation system as a mechano-nitrogenous fertilizer supplier. After driving the system by human walking stimuli, the $NaNO_3$ fertilizer is produced to benefit the growth of green beams. This work provides a feasibility to develop an energy-saving, environmental-friendly, flexible, and safe nitrogen fixation route.

## 4. Experimental

*Fabrication of the TENG-microplasma nitrogen fixation system:*

(1) Fabrication of the TENG: Polyurethane foams with the thickness of 2 mm were purchased from Jiangsu Xinkaisheng Enterprise Development Co., Ltd, China. Ebonite sheet (Thickness: 600 μm) were purchased from NIKKO EBONITE mfg. co., ltd., Japan. They were employed as the friction layer of the TENG without further treatment. The contact-separation mode TENG was fabricated by confronting the two frictional layers (5 cm × 5 cm) against each other. Nickel fabric and polycarbonate were successively attached on the rear sides of the frictional layers as electrodes and supporting substrate, respectively. Four springs with length of 10 mm and diameter of 8 mm were fixed on the four corners of polycarbonate substrates via epoxy adhesive and shafts to hold a gap between friction layers. (2) *Fabrication of the microplasma discharge reactor:* The microplasma discharge reactor was a custom-made glass cylinder (Drummond Scientific, Φ outer 5 cm, Φ inner 4.6 cm) with two stainless steel needles located in the opposite side of the cylinder. The gap distance between the needles could be adjustable. The top end of the reactor was capped with a helmet to avoid dust or dirt polluting the interior of the reactor. DI water or weak sodium bicarbonate solution was added into the reactor for absorbing generated nitrogen oxide. *(3) Fabrication of the TENG-microplasma nitrogen fixation system:* The TENG-microplasma nitrogen fixation system was achieved by connecting the electrodes of TENG with the needle electrodes of the microplasma discharge reactor.

*Measurements and Characterization:*

The TENG was driven by a linear motor. The output voltage and current of the TENG were measured by LeCroy WaveRunner Oscilloscope (44MXI) with the probe resistance value of

50 MΩ and low noise current amplifier (Stanford Research Systems, SR570), respectively. The emission spectrum of the microplasma discharge driven by the TENG is recorded by Ocean optics USB 4000 spectrometer. The concentration of nitrogen dioxide was measured by using a gas detector (EDKORS ADKS-1). The nitrate concentration in the range of 0-2000 ppm was detected by a spectrograph (HORIBA, LAQUAtwin-NO3-11).

*Green bean germination and growth*:

Green bean seeds were cultivated in Petri dishes at 28 °C in darkness for three days. Afterwards, uniform seedlings were transferred and placed in an incubator with DI water for growth with climate control. Continuous $NaNO_3$ solution was supplied to five green bean samples, while only DI water was supplied to the reference samples. After the growth for one week, the fresh weight of total biomass was measured for evaluating the growth rate of samples.

**Acknowledgements**

The research was supported by the grants from Research Grants Council of Hong Kong (GRF No. PolyU 153023/18P) and PolyU Grant (1 - ZVGH).

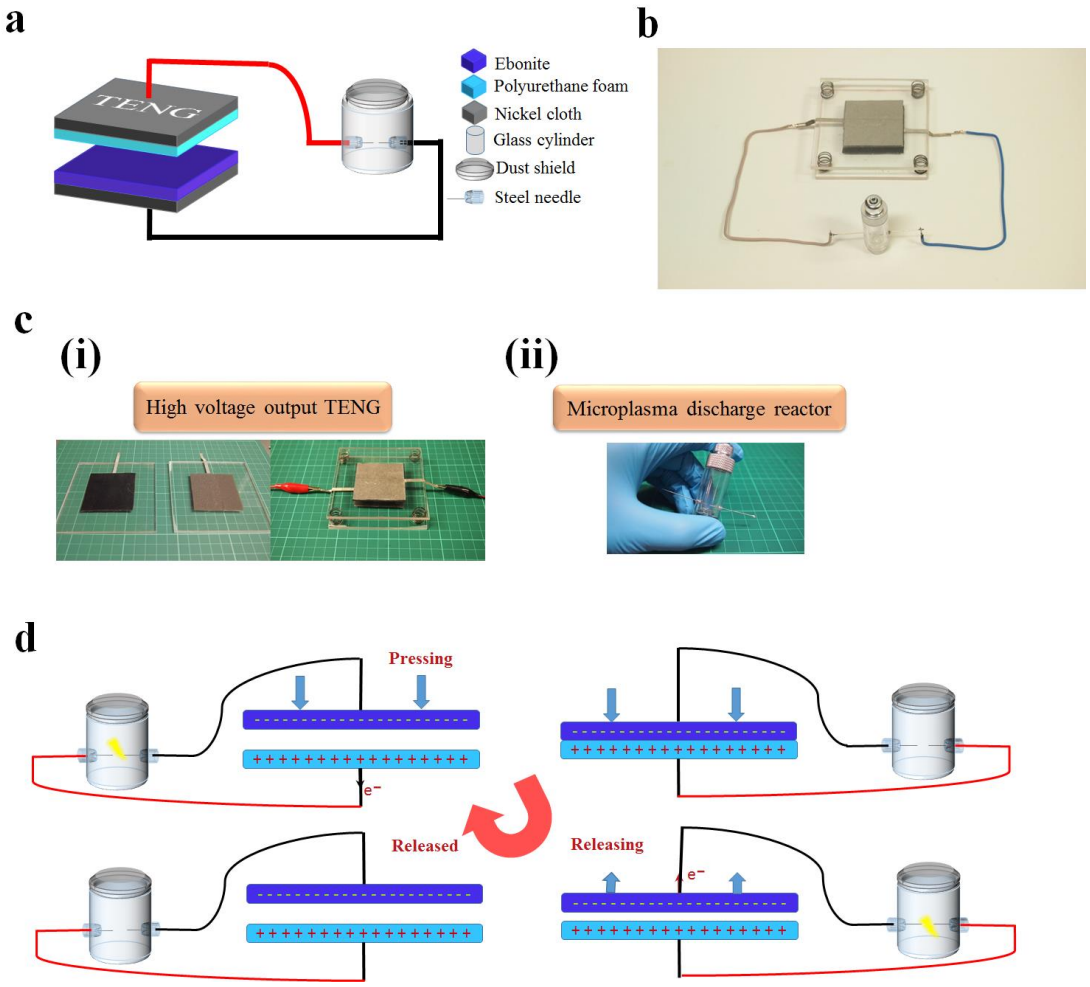


**Figure 1.** Illustration of TENG-microplasma discharge system (a) Schematic and (b) photographs of TENG-microplasma discharge system. (c) Photograph of the (i) TENG and (ii) microplasma discharge reactor. (d) Schematic of the working mechanism of the TENG-microplasma nitrogen fixation system.

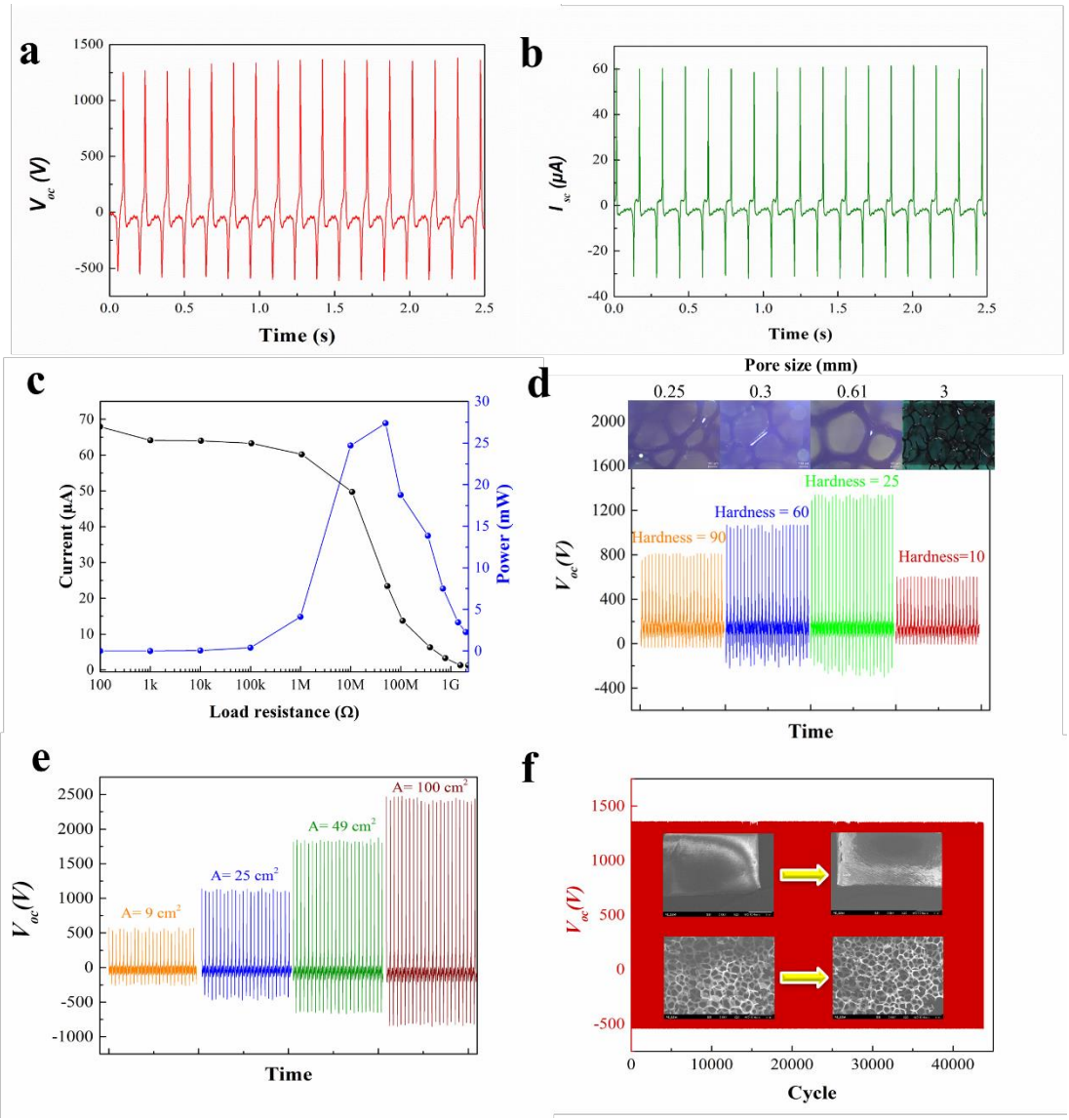


**Figure 2**. Electric performance of the high voltage TENG (a) Open-circuit voltage and (b) short-circuit current generated by TENG. (c) Dependence of the peak instantaneous current and peak instantaneous power of TENG on the external load resistance. (d) Open-circuit voltage of TENG versus the pore size of utilized PU foam friction material. (Inserts are the optical images of the PU foams with different pore size). (e) Open-circuit voltage of TENG under different frictional layer sizes. (f) The open-circuit voltage of the TENG after continuous operation for 45000 cycles at 7 Hz. Inserts are the SEM images of the two frictional layers before and after the operating process.

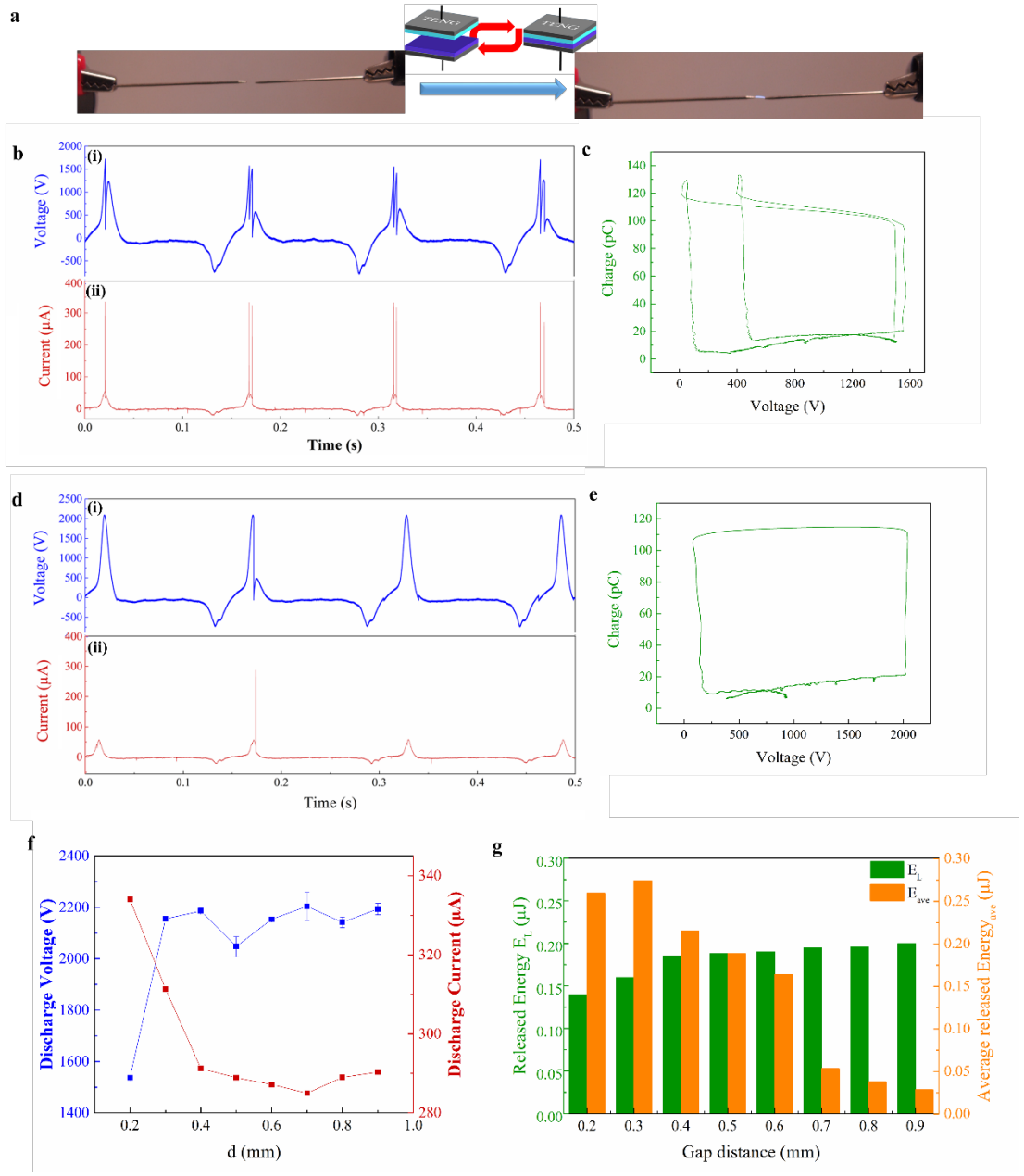


**Figure 3.** TENG driven microplasma discharge characterization (a) Photograph of the TENG-driven microplasma discharge between needle electrodes. (b) Change in voltage (i) and current (ii) between needle electrodes during four operation cycles of TENG. Gap distance between needle electrodes is 0.2 mm. (c) Lissajous figures of the microplasma discharge process with the gap distance of 0.2 mm. (d) Change in voltage (i) and current (ii) between needle electrodes during four operation cycle of TENG. Gap distance between needle electrodes is 0.6 mm. (e) Lissajous figures of the microplasma discharge process with the gap distance of 0.6 mm. (f) The discharge voltage and discharge current under different gap distance between needle electrodes. (g) The released energy for each microplasma discharge and the average discharge energy in each TENG operation cycle under different gap distance.

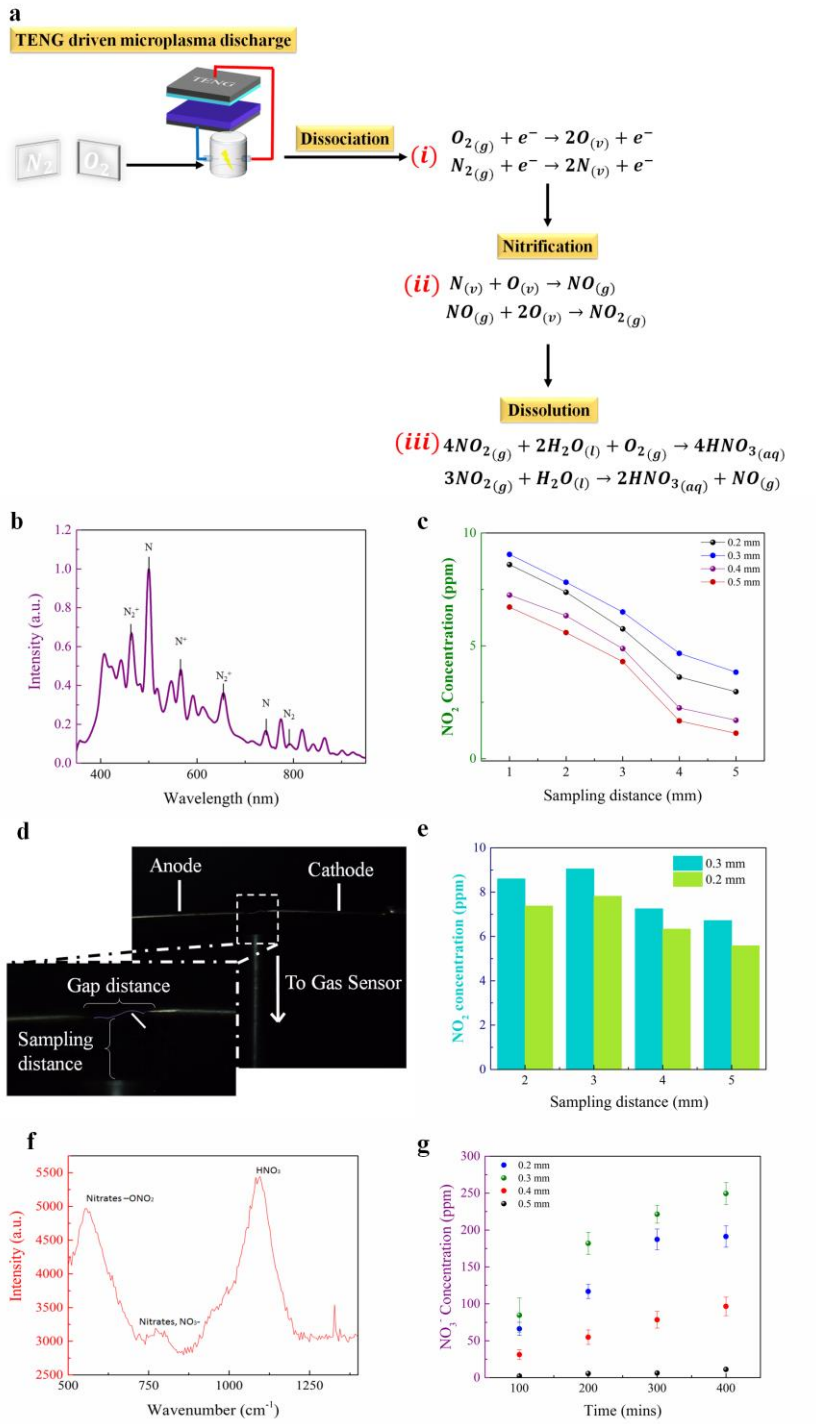


**Figure 4.** TENG driven nitrogen fixation characterization (a) Schematic of the conversion from nitrogen and oxygen molecules to nitrogen dioxide and nitric acid in TENG-microplasma nitrogen fixation system. (b) The emission spectrum of microplasma discharge. (c) The concentration of nitrogen dioxide detected under different sampling distance. (d) Schematic for nitrogen dioxide concentration measurement based on the EDKORS ADKS-1 gas detector. (e) The concentrations of nitrogen dioxide generated by microplasma discharge with different gap distance. (f) Raman spectrum of the prepared nitric acid solution in discharge reactor. (g) The nitrate concentration in nitric acid solution detected at the different operation time of TENG-microplasma nitrogen fixation system.

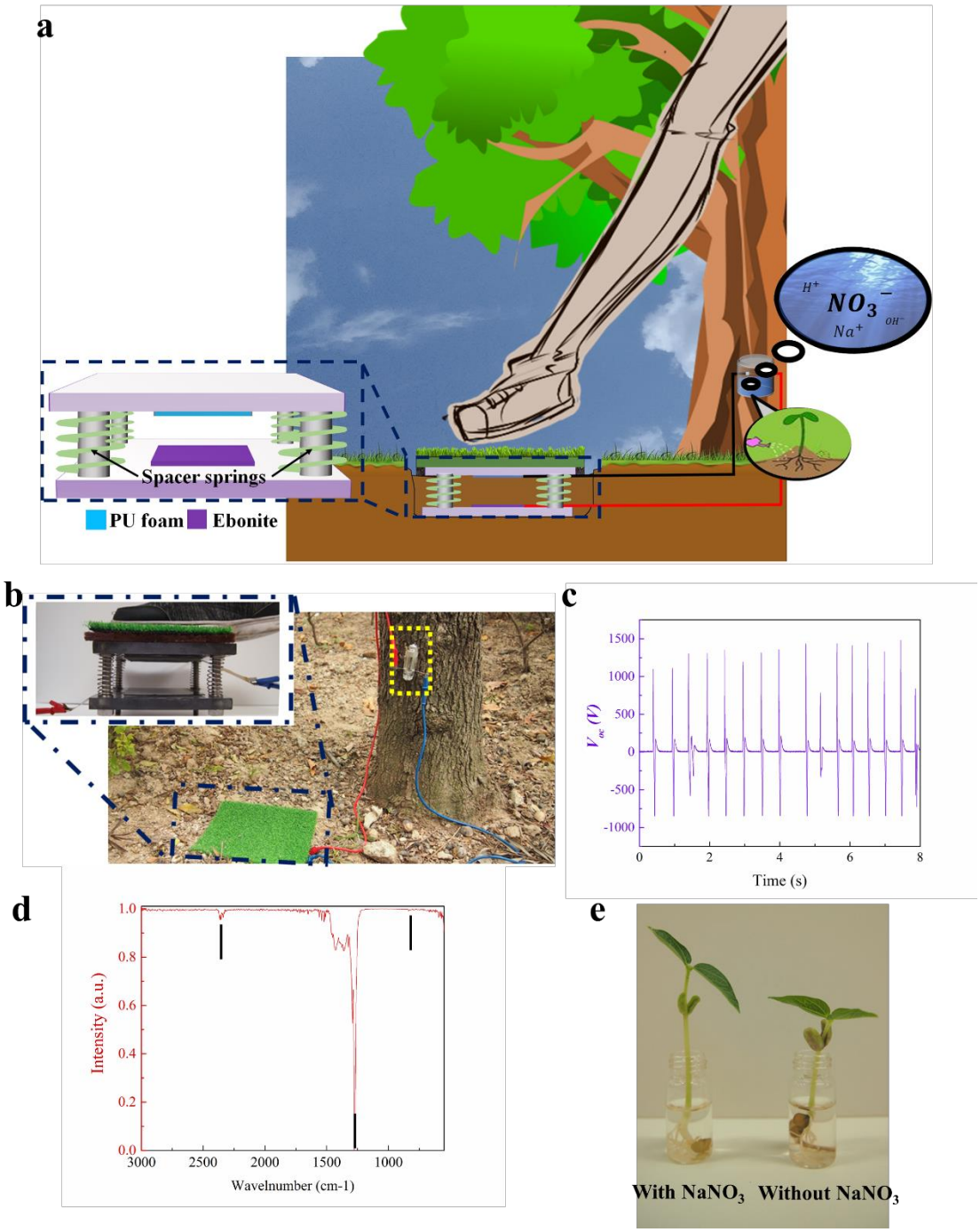


**Figure 5.** Demonstration of TENG microplasma discharge-based nitrogen fixation towards self-powered mechano-nitrogenous fertilizer supplier (a) Schematic and (b) Photograph demonstrating the setup of TENG-microplasma nitrogen fixation system as nitrogenous fertilizer supplier. (c) Open-circuit voltage generated by the buried TENG driven by human walking. (d) FTIR spectrum of the prepared $NaNO_3$ solution. (e) Comparison in growth rates between green bean samples with and without $NaNO_3$ addition.

**Table 1.** Comparison between traditional nitrogen fixation methods with the TENG-microplasma nitrogen fixation. [50, 56-59]

| Methods | Energy source | Raw materials | Synthetization Condition | Site of Synthetization | Product | Emission |
|---|---|---|---|---|---|---|
| **The Haber–Bosch process** | Fossil fuel | Natural gas, air, $K^+$, $Fe^{3+}$ catalyst etc. | High pressure, high temperature | Centralized | Ammonia | Carbon dioxide |
| **Biological nitrogen Fixation** | Adenosine triphosphate (ATP), sugar | Microbial organisms with nitrogenase enzymes | Ambient temperature and pressure | Depends | Ammonia | Adenosine diphosphate (ADP), Inorganic phosphate, etc. |
| **Metallocomplex nitrogen fixation** | Chemical energy | Strong metal reducing agents and transition metal complexes | Ambient temperature and pressure | Depends | Ammonia | Nil |
| **Plasma based nitrogen fixation** | Fossil fuel, renewable energy e.g. wind, solar, etc. | Air, water | Depends | Centralized | Nitric oxide | Nil |
| **TENG-microplasma nitrogen fixation** | Wasted or renewable mechanical energy | Air, water | Ambient environment | *In-situ* | Nitrogenous fertilizer | Nil |

## Reference


[1] W. Qiu, X.-Y. Xie, J. Qiu, W.-H. Fang, R. Liang, X. Ren, X. Ji, G. Cui, A. M. Asiri, G. Cui, B. Tang, X. Sun, *Nat. Commun.* **2018**, 9, 3485.

[2] N. Glock, Z. Erdem, K. Wallmann, C. J. Somes, V. Liebetrau, J. Schönfeld, S. Gorb, A. Eisenhauer, *Nat. Commun.* **2018**, 9, 1217.

[3] W. Wang, B. Patil, S. Heijkers, V. Hessel, A. Bogaerts, *ChemSusChem* **2017**, 10, 2145.

[4] G. Petitpas, J. D. Rollier, A. Darmon, J. Gonzalez-Aguilar, R. Metkemeijer, L. Fulcheri, *Int. J. Hydrogen Energy* **2007**, 32, 2848.

[5] J. Yang, T. Li, C. Zhong, X. Guan, C. Hu, *J. Electrochem. Soc.* **2016**, 163, E288.

[6] P. Peng, P. Chen, M. Addy, Y. Cheng, Y. Zhang, E. Anderson, N. Zhou, C. Schiappacasse, R. Hatzenbeller, L. Fan, *Chem. Commun.* **2018**, 54, 2886.

[7] M. A. Malik, C. Jiang, R. Heller, J. Lane, D. Hughes, K. H. Schoenbach, *Chem. Eng. J.* **2016**, 283, 631.

[8] Z. L. Wang, *Sci. Am.* **2008**, 298, 82.

[9] Z. L. Wang, *Mater. Today* **2017**, 20, 74.

[10] F. R. Fan, W. Tang, Z. L. Wang, *Adv. Mater.* **2016**, 28, 4283.

[11] W. Xu, M.-C. Wong, J. Hao, *Nano Energy* **2019**, 55, 203.

[12] L. B. Huang, G. Bai, M. C. Wong, Z. Yang, W. Xu, J. Hao, *Adv. Mater.* **2016**, 28, 2744.

[13] Z. L. Wang, *ACS Nano* **2013**, 7, 9533.

[14] Z. Liu, H. Li, B. Shi, Y. Fan, Z. L. Wang, Z. Li, *Adv. Funct. Mater.* **2019**, 29, 1808820.

[15] W. Xu, L.-B. Huang, J. Hao, *Nano Energy* **2017**, 40, 399.

[16] L. B. Huang, W. Xu, J. Hao, *Small* **2017**, 13, 1701820.

[17] P. Wang, L. Pan, J. Wang, M. Xu, G. Dai, H. Zou, K. Dong, Z. L. Wang, *ACS Nano* **2018**, 12, 9433.

[18] C. Wu, H. Tetik, J. Cheng, W. Ding, H. Guo, X. Tao, N. Zhou, Y. Zi, Z. Wu, H. Wu, D. Lin, Z. L. Wang, *Adv. Funct. Mater.* 0, 1901102.

[19] W. Xu, M.-C. Wong, Q. Guo, T. Jia, J. Hao, *J. Mater. Chem. A* **2019**, 7, 16267.

[20] H. Guo, Z. Wen, Y. Zi, M. H. Yeh, J. Wang, L. Zhu, C. Hu, Z. L. Wang, *Adv. Energy Mater.* **2016**, 6, 1501593.

[21] A. Ahmed, Z. Saadatnia, I. Hassan, Y. Zi, Y. Xi, X. He, J. Zu, Z. L. Wang, *Adv. Energy Mater.* **2017**, 7, 1601705.
[22] Y. Feng, Y. Zheng, G. Zhang, D. Wang, F. Zhou, W. Liu, *Nano Energy* **2017**, 38, 467.
[23] C. K. Jeong, K.-I. Park, J. H. Son, G.-T. Hwang, S. H. Lee, D. Y. Park, H. E. Lee, H. K. Lee, M. Byun, K. J. Lee, *Energy Environ. Sci.* **2014**, 7, 4035.
[24] Y. Feng, L. Zhang, Y. Zheng, D. Wang, F. Zhou, W. Liu, *Nano Energy* **2019**, 55, 260.
[25] Y. Wang, Y. Yang, Z. L. Wang, *NPJ Flexible Electron.* **2017**, 1, 10.
[26] L. B. Huang, W. Xu, G. Bai, M.-C. Wong, Z. Yang, J. Hao, *Nano Energy* **2016**, 30, 36.
[27] Z. Tian, J. He, X. Chen, Z. Zhang, T. Wen, C. Zhai, J. Han, J. Mu, X. Hou, X. Chou, C. Xue, *Nano Energy* **2017**, 39, 562.
[28] C. Wu, R. Liu, J. Wang, Y. Zi, L. Lin, Z. L. Wang, *Nano Energy* **2017**, 32, 287.
[29] W. Xu, L.-B. Huang, M.-C. Wong, L. Chen, G. Bai, J. Hao, *Adv. Energy Mater.* **2017**, 7, 1601529.
[30] P. Bai, G. Zhu, Z.-H. Lin, Q. Jing, J. Chen, G. Zhang, J. Ma, Z. L. Wang, *ACS Nano* **2013**, 7, 3713.
[31] Z. Wen, M.-H. Yeh, H. Guo, J. Wang, Y. Zi, W. Xu, J. Deng, L. Zhu, X. Wang, C. Hu, L. Zhu, X. Sun, Z. L. Wang, *Science Advances* **2016**, 2, e1600097.
[32] S. Niu, X. Wang, F. Yi, Y. S. Zhou, Z. L. Wang, *Nat. Commun.* **2015**, 6, 8975.
[33] C. Wu, A. C. Wang, W. Ding, H. Guo, Z. L. Wang, *Adv. Energy Mater.* **2019**, 9, 1802906.
[34] H. Kang, H. Kim, S. Kim, H. J. Shin, S. Cheon, J.-H. Huh, D. Y. Lee, S. Lee, S.-W. Kim, J. H. Cho, *Adv. Funct. Mater.* **2016**, 26, 7717.
[35] A. Li, Y. Zi, H. Guo, Z. L. Wang, F. M. Fernández, *Nat Nano* **2017**, 12, 481.
[36] C. Li, Y. Yin, B. Wang, T. Zhou, J. Wang, J. Luo, W. Tang, R. Cao, Z. Yuan, N. Li, X. Du, C. Wang, S. Zhao, Y. Liu, Z. L. Wang, *ACS Nano* **2017**, 11, 10439.
[37] H. Fang, H. Tian, J. Li, Q. Li, J. Dai, T.-L. Ren, G. Dong, Q. Yan, *Nano Energy* **2016**, 20, 48.
[38] X. Y. Wei, X. Wang, S. Y. Kuang, L. Su, H. Y. Li, Y. Wang, C. Pan, Z. L. Wang, G. Zhu, *Adv. Mater.* **2016**, 28, 6656.
[39] J. Cheng, W. Ding, Y. Zi, Y. Lu, L. Ji, F. Liu, C. Wu, Z. L. Wang, *Nat. Commun.* **2018**, 9, 3733.
[40] F. Yang, M. Zheng, L. Zhao, J. Guo, B. Zhang, G. Gu, G. Cheng, Z. Du, *Nano Energy* **2019**, 60, 680.
[41] C. Zhai, X. Chou, J. He, L. Song, Z. Zhang, T. Wen, Z. Tian, X. Chen, W. Zhang, Z. Niu, C. Xue, *Applied Energy* **2018**, 231, 1346.
[42] S. Wang, Y. Xie, S. Niu, L. Lin, C. Liu, Y. S. Zhou, Z. L. Wang, *Adv. Mater.* **2014**, 26, 6720.
[43] J. Wang, C. Wu, Y. Dai, Z. Zhao, A. Wang, T. Zhang, Z. L. Wang, *Nat. Commun.* **2017**, 8, 88.
[44] G. Cheng, H. Zheng, F. Yang, L. Zhao, M. Zheng, J. Yang, H. Qin, Z. Du, Z. L. Wang, *Nano Energy* **2018**, 44, 208.
[45] F. Liu, Y. Liu, Y. Lu, Z. Wang, Y. Shi, L. Ji, J. Cheng, *Nano Energy* **2019**, 56, 482.
[46] S. L. Zhang, Y. C. Lai, X. He, R. Liu, Y. Zi, Z. L. Wang, *Adv. Funct. Mater.* **2017**, 27, 1606695.
[47] H. Zhang, Y. Lu, A. Ghaffarinejad, P. Basset, *Nano Energy* **2018**, 51, 10.
[48] V. Babrauskas, presented at Proc. Interflam **2013**.
[49] R. Burlica, M. J. Kirkpatrick, B. R. Locke, *J. Electrostatics* **2006**, 64, 35.
[50] V. Hessel, A. Anastasopoulou, Q. Wang, G. Kolb, J. Lang, *Catal. Today* **2013**, 211, 9.
[51] B. Eliasson, U. Kogelschatz, *IEEE transactions on plasma science* **1991**, 19, 1063.
[52] N. Cherkasov, A. O. Ibhadon, P. Fitzpatrick, *Chemical Engineering and Processing:*

*Process Intensification* **2015**, 90, 24.
[53] V. K. Ahluwalia, *Advanced Environmental Chemistry*, Energy and Resources Institute, **2017**.
[54] N. Minogue, E. Riordan, J. R. Sodeau, *J. Phys. Chem. A* **2003**, 107, 4436.
[55] M. Trivedi, A. Branton, D. Trivedi, G. Nayak, K. Bairwa, S. Jana, *Journal of Chromatography & Separation Techniques* **2015**, 6.
[56] T. Shima, Z. Hou, in *Nitrogen Fixation*, Springer **2017**, p. 23.
[57] A. Mhaske, J. Gawad, C. Bonde, *Sci Revs Chem Commun* **2017**, 7, 102.
[58] J. Chatt, J. R. Dilworth, R. L. Richards, *Chem. Rev.* **1978**, 78, 589.
[59] F. Salvagiotti, K. G. Cassman, J. E. Specht, D. T. Walters, A. Weiss, A. Dobermann, *Field Crops Res.* **2008**, 108, 1.